Ultrafast Laser Ablation – A Peerless Synthesis Strategy for Functional Nanomaterials

Parvathy Nancy, Mohamed Nawas Vengoli, Sabu Thomas, Rodolphe Antoine, Nandakumar Kalarikkal

Ultrafast Laser Ablation – A Peerless Synthesis Strategy for Functional Nanomaterials

Parvathy Nancy[1,5], Mohamed Nawas vengoli[1,5], Sabu Thomas[1,3], Rodolphe Antoine[4], Nandakumar Kalarikkal[1,2,5]

[1]*International and Inter University Center for Nanoscience and Nanotechnology, Mahatma Gandhi University,*
[2]*School of Pure and Applied Physics, Mahatma Gandhi University, Kottayam 686560, Kerala, India*
Kottayam686560, Kerala, India
[3]*School of Nanoscience and Nanotechnology, Mahatma Gandhi University, Kottayam 686560, Kerala, India*
[4]*Institut Lumière Matière, UMR 5306 CNRS, Université Claude Bernard Lyon 1, Domaine Scientifique de La Doua, Batiment Kastler, 10 rue Ada Byron, 69622 Villeurbanne CEDEX, France*
[5]*University Centre for Ultrafast Studies, Mahatma Gandhi University, Kottayam 686560, Kerala, India*

Abstract

Ultrafast Laser Ablation Synthesis technique offers a rapid, straightforward, and eco-friendly approach for producing functional nanomaterials in comparison to alternative methods like colloidal chemistry. While previous studies on this have primarily focused on synthesizing nanomaterials and characterizing their structures and properties, there remains a significant gap in our understanding of the underlying physical processes that occur during ablation and material formation under extreme conditions. In particular, obtaining experimental data on transient parameters such as temperature and pressure during ablation possess significant challenges. As a result, there is a growing interest in on-going research efforts aimed at unravelling the formation mechanisms of a variety of functional nanomaterials and exploring their potential applications. Femtosecond laser offers a significant advantage in its capacity to generate nanostructures through a limitless array of solid targets and liquid mediums in a 'green' way. This chapter outlines the proficiency of femtosecond laser ablation as a fundamental technique for producing nanoscale assemblies comprising various functional materials, which exhibit intriguing physical and chemical properties.

1. Introduction

Laser ablation is a highly effective technology widely acknowledged for its capability in conducting direct chemical analysis of solid samples. In most cases, it eliminates the need for prior sample preparation, enabling swift analysis of elemental and isotopic composition. There are two main approaches for quantifying the ablated mass: one involves measuring the photons emitted by the optically induced plasma at the sample surface, while the other entails entraining the ablated aerosol into a gas stream and delivering it to a secondary source. Laser-induced breakdown spectroscopy (LIBS) and laser-ablation molecular isotopic spectroscopy (LAMIS) rely on optical emission measurements in the plasma (1–10). On the other hand, inductively coupled plasma (ICP) coupled with mass spectrometry (MS) or optical emission spectroscopy (OES) methods are based on

transporting the ablated aerosol [11–21)]. Although the sampling process remains consistent (via laser ablation), the choice of detection method is contingent upon the specific applications.

Laser ablation finds widespread applications beyond chemical analysis, including cutting, welding, micromachining, and LASIK surgery. Despite the varied fields, the core objective remains consistent: efficiently utilizing laser energy to remove material. Over the past five decades, extensive research has scrutinized nearly every factor influencing the ablation process. This process depends on a crucial factor determining effective material removal: the duration of the laser pulse. The insights gleaned from both nanosecond and femtosecond ablation studies, with pertinent comments on chemical analysis, drawing from plasma generation and particle detection. Picosecond lasers are not extensively discussed due to their relative scarcity in this domain, as applications are primarily driven by the availability of commercially accessible lasers. Until roughly 15 years ago, nanosecond pulsed lasers predominated, supplanting longer-pulse alternatives [22]. Although there are early references to long-pulse laser ablation, it is largely owing to the advent of short-pulse lasers (nanosecond and femtosecond) that chemical analysis has become feasible. It's worth noting that much of pulsed laser ablation research is empirical, lacking a unified theory predicting ablated mass quantity, plasma chemistry, or aerosol properties resulting from an ablation event. Short-pulse laser ablation shows great potential due to its ability to remove material from surfaces with a low threshold. This process involves the rapid application of energy, causing solid material to transition into a volatile phase. One possible mechanism for this transformation involves explosive boiling, where the matter is rapidly heated near its critical point. For extremely brief laser pulses, additional non-thermal excitation pathways may also come into play [23].

1.1. Femtosecond Laser Ablation

Femtosecond laser ablation has garnered significant attention for its exceptional attributes, including rapidity, cleanliness, and high efficiency [24, 25]. When femtosecond pulses are directed towards the target, they lead to multiphoton-absorption ionization, resulting in the formation of a plasma plume in an environment characterized by high temperature and pressure [26, 27]. In these extreme conditions, nanoparticles are generated through Coulombic explosion, accompanied by simultaneous surface functionalization. Consequently, femtosecond laser ablation stands as a convenient technique for producing various nanoparticles, encompassing iron oxide magnetic nanoparticles, alloy nanoparticles, and carbon dots [28-35]. In contrast to bottom-up synthetic approaches, the laser ablation method offers environmental benefits by reducing the reliance on chemical ligands and minimizing the residues of reducing agents. Moreover, the rapid transformation of particles into nanostructures via laser ablation (typically within tens of minutes) suggests that this method for preparing TMDs nanoparticles is more time-efficient compared to top-down techniques like solvothermal approaches[36].

1.2. Fundamentals

To remove an atom from a solid using a laser pulse, it is necessary to deliver energy exceeding the atom's binding energy. Consequently, when ablating the same amount of material with a short laser pulse, one must apply higher laser intensity, which is inversely proportional to the pulse duration. For instance, laser ablation with 100 femtosecond (fs) pulses requires an intensity in the range of approximately 10^{13} to 10^{14} W/cm², while ablation with 30-100 nanosecond (ns) pulses can be achieved at intensities around 10^{8} to 10^{9}W/cm² [37, 38]. At intensities above 10^{13} to 10^{14} W/cm², ionization of virtually any target material occurs early in the laser pulse's duration. For example, when an intense femtosecond pulse at 10^{13} to 10^{14}W/cm² interacts with a dielectric material, nearly complete single ionization of the target happens at the beginning of the laser pulse. Following ionization, the laser energy is absorbed by free electrons through processes like inverse Bremsstrahlung and resonance absorption, and this absorption mechanism does not depend on the initial state of the target material. Therefore, the interaction with both metals and dielectrics proceeds similarly when using ultra-short laser pulses, in contrast to the situation with long pulses, where ablation of metals occurs at relatively low intensity compared to transparent dielectrics with negligible absorption. Another distinguishing characteristic of ultra-short laser interaction is that the energy transfer time from electrons to ions due to Coulomb collisions is significantly longer, on the order of picoseconds, than the laser pulse duration, which is typically around 100 femtoseconds. As a result, conventional hydrodynamics motion does not occur during the femtosecond interaction period.

Momentum transfer from the laser field and energetic electrons to ions in the absorption zone is governed by two primary forces: the electric field of charge separation and the ponderomotive force. When the energy absorbed by electrons surpasses the Fermi energy, which is a combination of binding energy and work function, it enables electrons to escape from the target. The electric field resulting from charge separation then pulls ions out of the target. Simultaneously, the ponderomotive force generated by the laser field in the skin layer propels electrons further into the target, facilitating ion acceleration within the target material. It is noteworthy that in the context of sub-picosecond laser pulses with intensities ranging from 10^{13} to 10^{14}W/cm², the former mechanism predominantly governs the ablation process, differentiating it significantly from thermal ablation induced by longer pulses.

Femtosecond ablation is notably sensitive to both the temporal and spatial variations in the laser pulse intensity. The Chirped Pulse Amplification (CPA) technique, frequently employed for generating short laser pulses, can yield a primary short pulse accompanied by a nanosecond pre-pulse or pedestal [39]. This pre-pulse, in some cases, can be sufficiently intense to initiate target ablation on its own. Therefore, for practical implementation of a pure femtosecond interaction mode, it is imperative to ensure that the intensity of any pre-pulse remains below the thresholds for ablation or ionization characteristic of the nanosecond regime. Fortunately, several methods, such as the use of nonlinear absorbers and second harmonic conversion, can be employed to achieve high pulse contrast and meet these criteria [40, 41].

Femtosecond laser ablation yields distinct physical characteristics compared to nanosecond laser ablation, particularly due to the ultra-short pulse duration, which is on the

order of femtoseconds. One critical factor to consider is the relaxation time associated with electron-phonon interactions, typically in the picosecond range. When a femtosecond laser is focused on a bulk material's surface, the initial photon energy is rapidly absorbed by the electrons, leading to a significant increase in electron thermal motion and temperature. However, because of the extremely brief pulse duration, there is insufficient time for the electrons to transfer this energy to the lattice (or ions). Consequently, the electron subsystem attains a very high temperature, while the lattice subsystem remains relatively cool. This results in what is often referred to as a 'cold' ablation process.

In general, the thermal equilibrium time for metals is typically a few femtoseconds, whereas it is in the order of nanoseconds for semiconductors or insulators. This difference is primarily attributed to the variation in energy band gaps. The larger the energy gap, the longer it takes for excited electron-hole pairs to reach thermal equilibrium through processes like generation-recombination. Within the short pulse duration, two distinct temperature subsystems exist within the target: the electronic subsystem and the lattice subsystem. These subsystems are typically described using two coupled thermal conduction equations representing electron-phonon coupling, collectively known as the two-temperature model for femtosecond laser ablation.

In contrast to long-pulse laser ablation (LPLA), femtosecond laser ablation primarily relies on mechanisms such as multiphoton ionization or tunneling ionization to generate electrons. In this context, the presence of dopants and defects within the lattice has a relatively minor impact on the generation-recombination of electron and vacancy pairs. Consequently, for femtosecond laser ablation, the ablation thresholds for different materials tend to be similar. When considering lasers with the same energy density and repetition frequency, those with shorter pulse widths and higher peak power are better suited to meet the ablation threshold of the target material.

The absorption of laser energy within a material occurs within a very short distance (approximately 10 nm), leading to a rapid increase in electron temperature, plasma density, and pressure. In insulators, high-energy electrons, generated by both thermal excitation and multiphoton photoelectric processes, are expelled from the irradiated surface, creating a strong electric field (around 1011 V/m) between the surface and the electron cloud. This field persists for up to 1 picosecond [42-44]. In this electrostatic environment, ions can be ejected from the surface through Coulomb explosion, contributing to the rapid removal of material layers in dielectrics. In contrast, in metals and semiconductors, this process is less significant. Free electrons in these materials quickly redistribute through diffusion and drift processes [45].

The heating rate of electrons by the laser governs the rates of excitation and ionization. The time it takes for the electrons to elevate the material's temperature to a high level is on the order of tens of femtoseconds. This leads to the transformation of solid material into plasma, provided that the laser power density reaches around 10^12 (10^{12}) Watts/cm^2The hot electrons then thermally interact with the ions and lattice through electron-phonon coupling within 10–100 picoseconds, resulting in localized temperature increase. The

energy deposition occurs so rapidly that the material cannot evaporate continuously, leading to the build-up of extremely high temperature and pressure beneath the evaporating surface. This sets off a breakdown of the irradiated volume, ejection of atomic clusters through Coulomb explosion, and the emergence of plasma from the ablation plume [46-48]. Due to swift and isochoric heating, the temperature surges to as high as 10,000 K, followed by an adiabatic expansion of the plasma volume. As the plume expands, it cools down due to adiabatic expansion. The laser-induced plasma undergoes various stages during this expansion, facilitating particle generation from the vapour phase. The entire ablation process can extend over several microseconds, especially in the second ablation phase triggered by nucleation, whether heterogeneous or homogeneous. This delay is attributed to the time required for nucleation bubbles to form and grow. Several intermediate thermodynamic pathways are observed, influenced by factors such as pulse energy and energy distribution within the irradiated volume, including vaporization, fragmentation, phase explosion, and spallation [50-53].

In the case of nanosecond laser radiation (around 10^8 to $10^9 W/cm^2$), absorption is weaker and dependent on the material's chemical and physical properties. Absorption typically occurs through inter-band transitions, defects, and excitations. In this long-pulse ablation mode, the electron-to-lattice energy exchange happens much faster than the pulse duration, resulting in partial buffering of pulse energy through plasma-light interactions. The remaining energy is primarily consumed by heat diffusion. As a result, electrons and ions reach equilibrium, and ablation is predominantly driven by thermal evaporation. In contrast, in nanosecond-laser ablation, melting takes precedence, and ablation occurs through hydrodynamic sputtering from surface instabilities like Rayleigh–Taylor and Kelvin–Helmholtz [54, 55]. Figure 1 (a) illustrates the phase transitions during sample irradiation by nanosecond laser, culminating in vaporization and plasma formation. Figure 1 (b) depicts a two-step ablation process involving the initial formation of hot electrons and a cold sample array, followed by electron heating and plasma explosion. Figures 1 (c) and (d) provide visual representations of the plasma plume resulting from surface irradiation by nanosecond and femtosecond lasers, respectively [56].

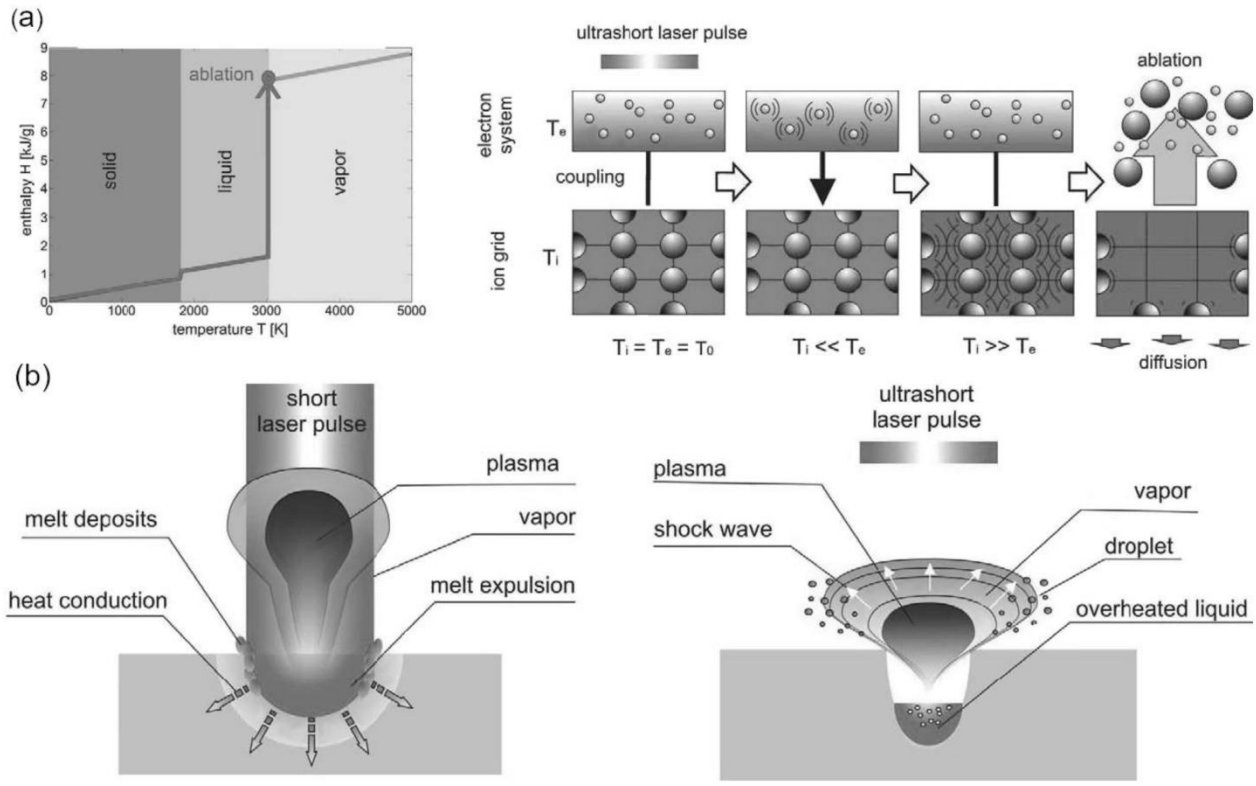

Figure 1. Ablation models encompass two key approaches: (a) the classical ablation model, and (b) the two-temperature model, which forms the foundation for the ultrafast ablation model. Regarding the interaction between a beam and matter, two distinct types are considered: (c) classical beam-matter interaction, and (d) ultrafast beam-matter interaction [56].

2. Synthesis of Functional Nanomaterials using Ultrafast Lasers

Over the past decade, functional nanomaterials have an astonishing impact on our daily lives. Progress in the nanomaterials science and its breakthrough developments are underpinned to a great extent by new smart advanced functional materials with outstanding properties. Within this context, extensive research efforts have been devoted to the design of new nano-devices based on their synthesis, engineering, and functionalization. These novel materials, notable for their extremely small feature size, i.e., from the atomic to nano-scale and further, have the potential for wide-ranging applications. These new generation high-performance materials have been attracting much attention due to their extraordinarily high synergetic and complementary behavior in the nano-level. To meet the fast growing performance demands (technological and industrial) like miniaturization and accuracy, synthesis of such materials require simultaneous advances. Hence future research explorations on ultrafast synthesis of novel nanomaterials will enhance the possibility of designing next generation unique nano- devices with high-level performance efficiency.

2.1. Liquid Phase Laser Ablation

Laser Ablation in Liquid (LAL) is an advanced technology known for its extremely rapid cooling capabilities (with a cooling rate of up to 10^{10} Ks^{-1}). It is widely utilized in the design and production of nanoparticles, leading to the synthesis of a significant number of unique metastable nanoparticles with distinctive properties in recent decades. The core principle of LAL involves using a high-energy laser to bombard and heat target materials in a liquid state. This process causes the local target material to melt into a metal droplet, and the high temperature leads to rapid evaporation of the surrounding liquid. The resulting explosion generates a momentary high pressure in the vicinity, and the force of this high-energy steam disperses the tiny metal droplet or plasma plume into the surrounding liquid, inducing a powerful quenching effect. As a result, metastable nanocrystals are formed, and the surrounding liquid transforms into a colloidal solution. According to researchers, the pressure and temperature within the bubble can reach as high as 10^7–10^8 Pa and up to 3,000 K, respectively [56-61]. The various forms of LAL technology, including millisecond, microsecond, nanosecond, femtosecond, and picosecond, are categorized based on different laser emission devices. Compared to other methods for synthesizing nanomaterials, LAL offers several advantages: (1) it is environmentally friendly, using simple raw materials without generating by-products or requiring catalysts; (2) it is versatile and applicable to a wide range of materials and solvents, enabling the synthesis of diverse forms of nanocrystals and holding great potential for nanomaterial development; (3) LAL can be conducted at room temperature; and (4) it allows for precise control over the phase, size, and shape of nanocrystals through specific auxiliary strategies or direct adjustment of laser parameters [62]. Given its potent quenching effect, laser technology holds immense promise in the field of nanomaterial synthesis. Such generated nanomaterials especially nanohybrid materials have multifunctional applications [63-67].

3. Femtosecond Laser Induced Synthesis Strategies

3.1. Generation of transition metal dichalcogenides (TMDs) quantum dots

Heavy metal-free quantum dots, transition metal dichalcogenides (TMDs) and boron nitride (BN) quantum dots (QDs), have garnered significant attention due to their desirable properties, such as excellent thermal conductivity, chemical stability, and unique optical characteristics. While various methods have been employed to synthesize TMDs, most of these methods are plagued by their time-consuming and complex nature, which restricts the potential applications of TMDs. Here, an expedited and straightforward approach for producing high-quality molybdenum disulfide (MoS_2) QDs and tungsten disulfide (WS_2) QDs are established. This method is based on the combined use of femtosecond laser ablation and sonication-assisted liquid exfoliation.

Tungsten disulfide (WS_2) and molybdenum disulfide (MoS_2) quantum dots (QDs) were synthesized using a two-step method involving femtosecond laser ablation and sonication-assisted liquid exfoliation in N-Methyl-2-pyrrolidone (NMP) as the solvent which is illustrated in figure 2. In the first step, bulk MoS_2 and WS_2 powders were subjected to femtosecond laser ablation, resulting in the formation of small multilayer

nanoparticles of MoS_2 and WS_2. Subsequently, these multilayer nanoparticles were further exfoliated into quantum dots (QDs) through ultrasonic treatment. After completing these two steps, the final product was faint yellow solutions containing MoS_2 and WS_2 QDs. The choice of NMP as the solvent was based on its ability to match the surface energy with the van der Waals forces of the MoS_2 and WS_2 layers, which facilitated the exfoliation of the multilayer nanoparticles into monolayer QDs [69].

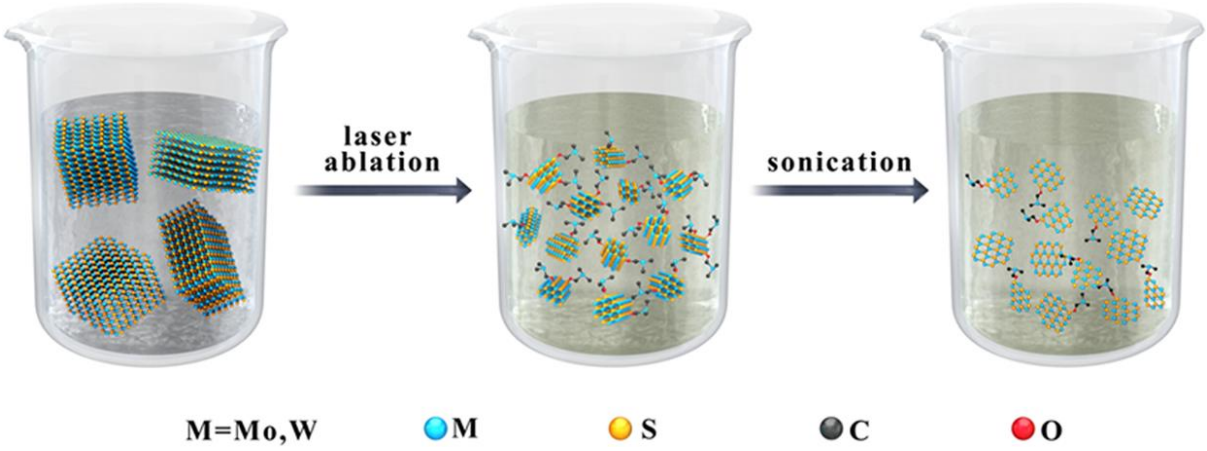

Figure 2. The process for synthesizing Transition Metal Dichalcogenides Quantum Dots (TMDs QDs) using a combination of femtosecond laser ablation and sonication-enhanced liquid exfoliation. [68]

Transmission electron microscopy (TEM) was employed to analyze the microstructure and size distribution of the MoS_2 and WS_2 quantum dots (QDs). The TEM samples were prepared by placing a small droplet of the TMDs QDs solution onto a copper grid with a thin, transparent carbon film. As depicted in 3(a) & (b) the average lateral dimensions of the MoS_2 and WS_2 QDs were approximately 3.7 nm and 2.1 nm, respectively. The high-resolution TEM (HRTEM) images in the inset of figure.3 (a) & (b) affirm the well-crystallized nature of both QDs. The measured d-spacing of the MoS_2 QDs was 0.19 nm, corresponding to the (105) facet of the MoS_2 crystal. Likewise, a lattice spacing of about 0.2 nm could be attributed to the (006) plane of the WS_2 crystal, confirming the identity of these QDs as either MoS_2 or WS_2 QDs [70, 71].

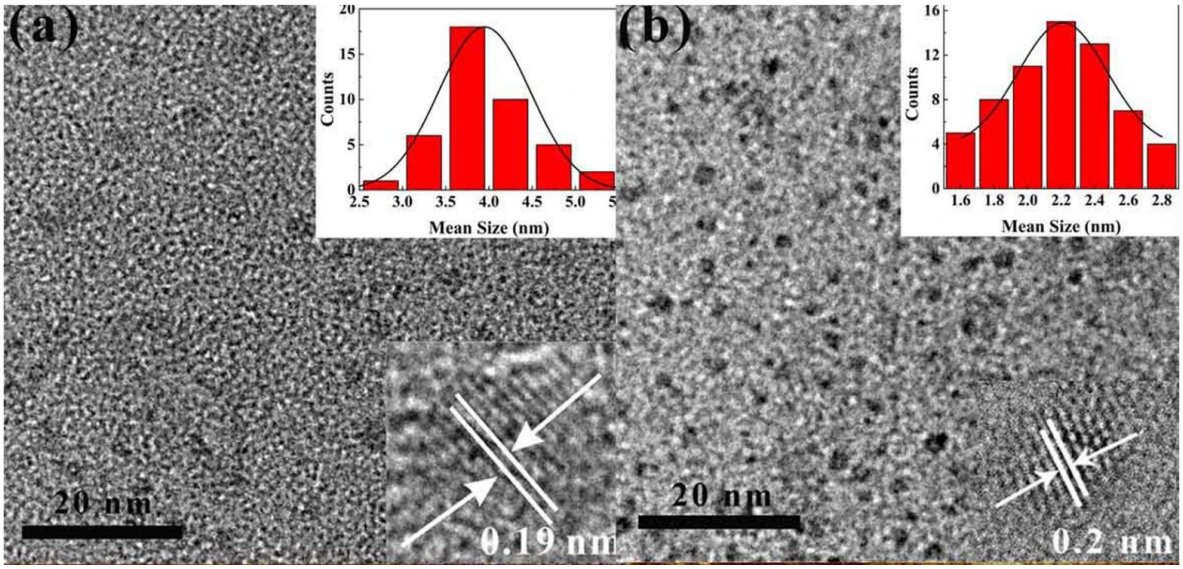

Figure 3 TEM & HRTEM images of the (a) MoS_2 and (b) WS_2 QDs [68].

.

Femtosecond laser ablation can be successfully employed to reduce bulk MoS_2 and WS_2 into minute nanoparticles, followed by an ultrasonic treatment to further exfoliate them into MoS_2 quantum dots (QDs) and WS_2 quantum dots (QDs). Additionally, this study presents an efficient, economical, and straightforward method for producing transition metal dichalcogenides QDs as well as other two-dimensional nanomaterials.

3.2. **Fabrication of Hybrid Nanoparticles**

A one-step and lithography-free laser-induced dewetting process of bi-layer nanoscale-thickness gold-silicon films on a glass substrate can be done using a femtosecond laser. This technique enables the creation of hybrid nanoparticles, highlighting their superior performance compared to simple metallic dielectric nanostructures, despite the traditionally challenging and time-consuming nature of their fabrication. Hybrid nanoparticles (NPs) are produced by utilizing a setup depicted in Figure 4, which is based on a commercially available femtosecond laser system. This system, the femtosecond oscillator TiF-100F from Avesta Project located in Troitsk, Moscow, Russia, emits light with a central wavelength of 790 ± 5 nm. The laser pulses have duration of 100 femtoseconds and are generated at a repetition rate (RR) of 80 MHz. The laser radiation is controlled by an acousto-optic modulator (AOM) and passes through a motorized attenuator, indicated by the dashed rectangle in Figure 4.

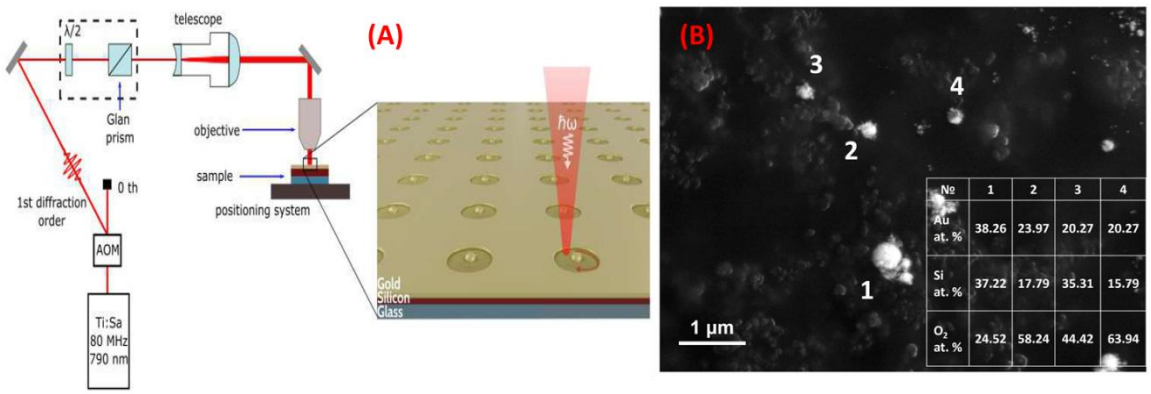

Figure 4. (a) The experimental arrangement employed for particle production is depicted, with an additional detail highlighting the creation of an array of hybrid nanoparticles through the precise laser ablation of a patch from a bilayer film composed of Au and Si, situated on a glass substrate (b) An image captured using High-angle Annular Dark Field Scanning Electron Microscopy (HAADF-SEM) displays hybrid nanoparticles [72]

Energy Dispersive X-ray (EDX) measurements of individual NPs (Figure 3) reveal the coexistence of gold and silicon atoms, along with oxygen and hence support support the hypothesis of a complex internal microstructure formation. Specifically, in the case of hybrid NPs produced from a 30/180 nm Au/Si film, the measurements indicate an average composition of 20.3 ± 7.3 atomic percent of gold and 25.4 ± 8.4 atomic percent of silicon, which is shown in figure 4 b. The accompanying legend in figure 4(b) provides the atomic percentage composition of gold and silicon, determined via Energy Dispersive X-ray Spectroscopy (EDX), at specific positions marked by numbers 1 to 4 [72]. This fabrication technique enables the production of sizable nanostructures, reaching diameters of up to 1 μm, while also allowing for accurate positioning.

3.3. Femtogels of Reduced Graphene Oxide

Ibrahim et al presented a groundbreaking technique is presented in this study for producing reduced graphene oxide gel at room temperature, without the need for any additional chemicals or agents [73]. This innovative process involves subjecting a highly concentrated solution of single-layer graphene oxide flakes to high-intensity femtosecond laser pulses. A high-intensity femtosecond laser, with pulse energy of 250 μJ, pulse duration of 100 fs, and a focal length of 5 cm, was used to irradiate an ultrahigh concentration aqueous solution of graphene oxide containing single-layer flakes ranging in size from 0.5 to 5 μ. The laser is precisely focused at the interface between the air and the aqueous solution, which enhances the vaporization of functional groups and water, ultimately leading to the formation of femtogel. By adjusting parameters such as pulsed laser intensity, beam focal characteristics, and pulse duration, it is possible to generate several milliliters of femtogel in as little as 8 minutes. The resulting material possesses physical and chemical properties akin to a monolayer graphene sheet.

A highly viscous femtogel is created by directing a femtosecond laser onto the surface of an extremely concentrated single-layer flake graphene oxide solution in water. This process eliminates hydroxyl and carboxyl functional groups, along with water molecules. Reduction of the graphene oxide and the formation of the gel happen simultaneously, taking only a few minutes at room temperature. This enables the production of compact, stratified thin films using the femtogel.

3.4. Nanodiamonds by femtosecond laser

Carbon nanomaterials, such as nanodiamonds, display unique attributes, encompassing improved thermal, electrical, mechanical, and biological characteristics. Initially identified in meteorites, nanodiamonds have been observed to possess biocompatibility, non-toxicity, and distinctive optical features. Nanodiamonds measuring less than 5 nm in size can be synthesized directly from ethanol through the application of a femtosecond laser with a wavelength of 1025 nm. The absorption of laser energy by ethanol exhibits a nonlinear increase beyond 100 microjoules, giving rise to a white light continuum due to the phenomenon of femtosecond laser filamentation.

In this experiment, 500 femtosecond (fs) laser pulses with a wavelength of 1025 nanometers (nm) and a repetition rate of 1 kilohertz (kHz) were focused into ethanol contained in a quartz cuvette. The setup is illustrated in Figure 5a, The critical power required for self-focusing in ethanol was calculated as an approximate value of 1.5 × 10^6 watts. By varying the laser energy from 10 microjoules (μJ) to 650 μJ, the laser power ranged from 10^7 to 10^9 watts, which is approximately 1 to 3 orders of magnitude higher than the critical power needed for self-focusing in ethanol. Figures 1b to 1e depict the side view of the fs laser irradiation captured by a CCD camera, with laser energies ranging from 180 to 626 μJ. As the laser energy increased, filaments were observed forming before the geometrical focus of the laser beam, resulting in a streak along the laser axis that was transmitted through the bottom of the quartz cell [74].

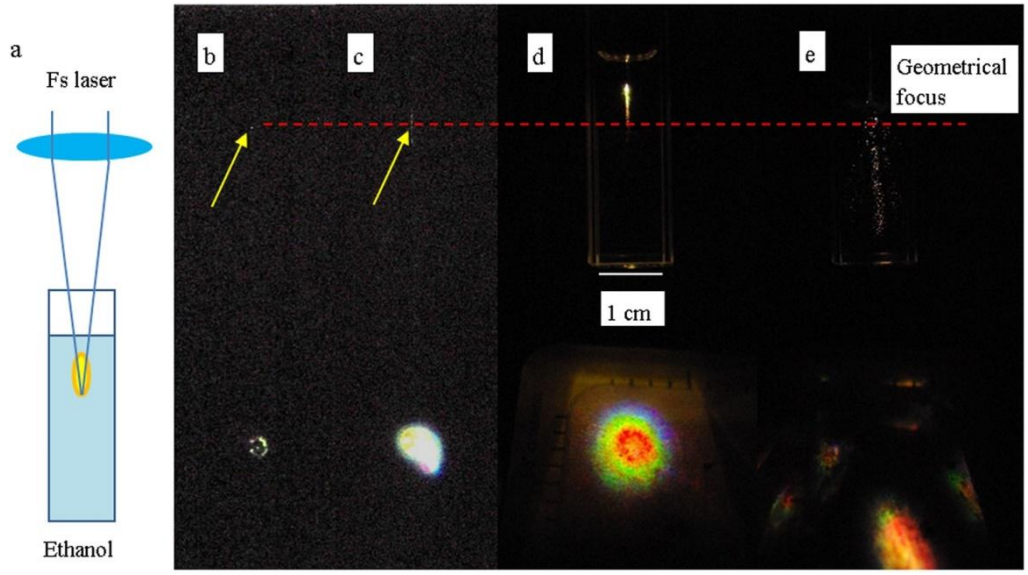

Figure 5 (a) experimental set up and effects of pulsed femtosecond (fs) laser exposure on ethanol from a side view. The incident laser energy levels are as follows: (b) 141 μJ, (c) 262 μJ, (d) 410 μJ, and (e) 626 μJ. The arrows indicate the spots where emission occurs, and the dotted line signifies the focal point of the laser beam. These images were captured using a shutter speed of 1/1000 second, while the laser operated at a repetition rate of 1 KHz [74].

3.5. **Monolayer MoS_2 Quantum Dots**

Utilizing temporally shaped femtosecond laser ablation in water represents an innovative, efficient, and one-step method for producing consistent monolayer MoS_2 quantum dot. These ultrashort-pulsed, high-intensity femtosecond lasers, with peak power densities exceeding 10^{13} W/cm^2, introduce nonthermal effects and nonlinear nonequilibrium processing, enabling the potential for monolayer photoexfoliation of two-dimensional materials. By employing temporally shaped femtosecond lasers, we can enhance MoS_2 nanomaterial production rates, particularly uniform, small MoS_2 quantum dots. This outcome arises from a blend of monolayer MoS_2 photoexfoliation and water-induced light absorption via photoionization, controllable through pulse shaping [75]. This approach offers notable benefits: significantly reduced preparation time, eco-friendliness by ablating bulk MoS_2 in water, yielding high-purity MoS_2 quantum dots without the need for metallic additives or chemical agents. The use of temporally shaped femtosecond lasers offers distinct advantages: it enables the creation of uniform monolayer MoS_2 quantum dots with a size range of 1–5 nm and produces high yields (36.73 wt%) of small monolayer MoS_2 quantum dots.

The experimental setup for temporally shaped femtosecond laser ablation is illustrated in Figure 6[6]. In this setup, a standard femtosecond pulse is transformed into two subpulses (with an energy ratio of 1:1 and a total laser fluence of 0.77 J/cm^2). These subpulses can be temporally separated within a time frame ranging from 0 to 10 ps. The mechanism involves multilevel photo exfoliation of monolayer MoS_2 and enhanced light absorption through water photoionization. This process is initiated and precisely regulated using a temporally shaped femtosecond laser, as depicted in Figure 6 [75].

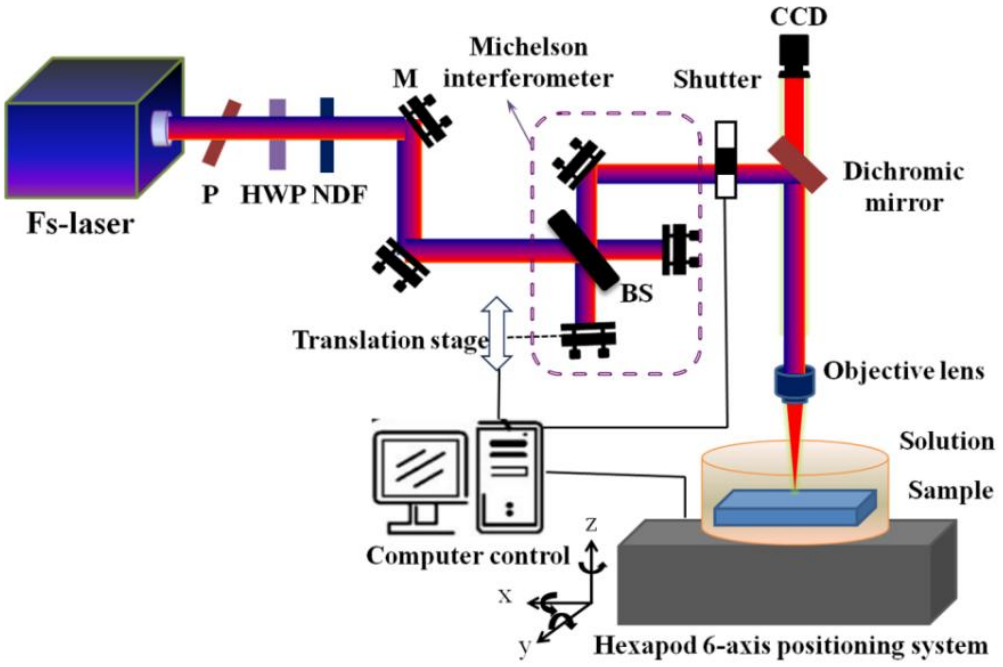

Figure 6: the setup for generating two subpulses. It includes components such as a polarizer (P), half-wave plate (HWP), neutral density filters (NDF), mirrors (M), beam splitter (BS), and charge-coupled device (CCD) [75].

When the first subpulse irradiates, electron-hole recombination lasts 2-100 ps. The second subpulse (10 ps delay) enhances Coulomb repulsion, leading to second-level photo exfoliation (small monolayer MoS_2 QDs). The first subpulse ionizes water molecules (200 fs to 13 ps) and boosts light absorption for the second subpulse, increasing MoS_2 QD yield. In single-pulse ablation, higher fluence results in thermal processes, yielding larger nanosheets/nanoparticles. Pulse shaping enhances MoS_2 nanomaterial production, favoring small, uniform MoS_2 QDs. Tailoring laser power and the delay between two subpulses within a pulse train allows for the creation of uniform-sized MoS_2 quantum dots with a heightened production rate. To further enhance production rates, exploring multi-beam parallel processing and optimizing laser parameters, such as scan speed, wavelength, and pulse delay, offers additional avenues.

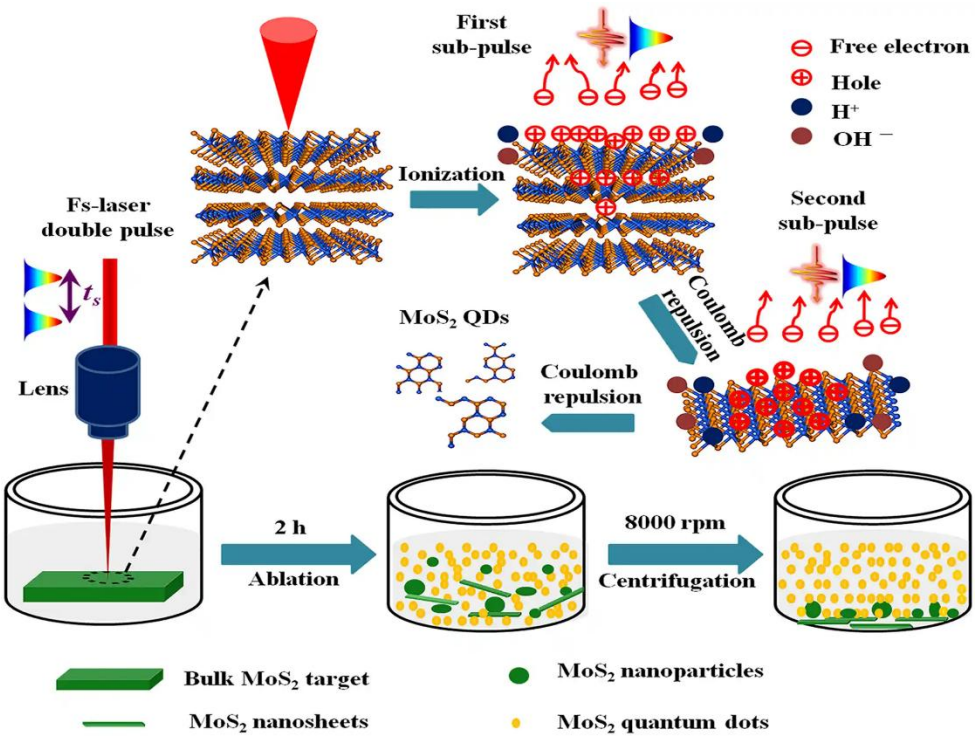

Figure 7: A schematic illustrating the process mechanism for ablating bulk MoS_2 targets in water using a temporally shaped femtosecond laser with a two-subpulse train [75].

3.6 . Twin Graphene quantum dots

Twin graphene has the capacity to induce enduring and extensive defects in energy band configurations, resulting in distinct electron transport characteristics [76]. These attributes hold promise for potential uses in magnetism, spin transport, and photoluminescence applications, fostering innovation and technological progress.
Electric-field-assisted temporally-shaped femtosecond laser ablation in a liquid (ETLAL) is employed to create graphene quantum dots (GQDs) featuring an average size of 2-3 nm and a surface modified with oxygen-containing functional groups. This innovative method enables the controlled synthesis of both single crystal and twin GQDs (5-fold twin). It achieves this by manipulating the crystallinity of GQDs in two ways: first, by applying an electric field to direct the motion of cavitation bubbles and nanoparticles, facilitating collision and crystallization at elevated temperatures and pressures, a key factor in twin GQD formation. Second, by adjusting the temporally-shaped femtosecond laser pulse delay, the proportion of Coulomb explosion during ablation can be controlled, increasing the carbon clusters provided by the cavitation bubble and influencing the polyploid nature of twin GQDs [76].

Monolayer or bilayer graphene quantum dots (GQDs) featuring controlled defects, uniformity, and small size (average size of 2-3 nm) were successfully produced using Electric-Field-Assisted Temporally-Shaped Femtosecond Laser Ablation in a Liquid (ETLAL) of graphene dispersion. The experimental setup for this process is depicted in Figure 8.

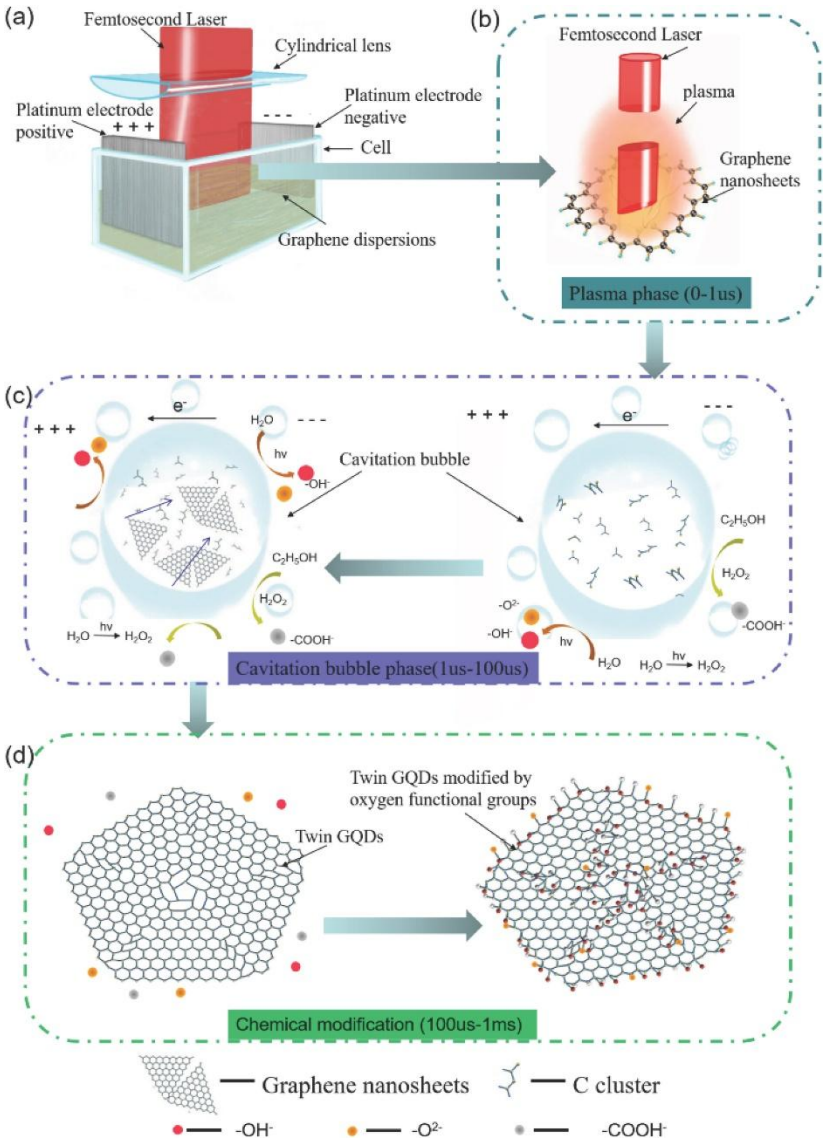

Figure 8: the schematic for the controlled preparation of twin graphene quantum dots (GQDs) through the Electric-Field-Assisted Temporally Shaped Femtosecond Laser Ablation in Liquid (ETLAL) of graphene dispersion. Schematic of experimental setup(a), the figure showcases different phases of the process, including the plasma phase (b), the cavitation bubble phase (c), and the chemical modification phase (d), Reproduced from Elsevier: Carbon with permission[76].

The plasma phase involves several rapid processes, including energy absorption by graphene nanosheets, ionization, electron heating, Coulomb explosion, and plasma formation[77]. The density of carbon clusters in the plasma, crucial for GQD formation, can be controlled by managing the dominance of Coulomb explosion during femtosecond laser ablation. Temporally-shaped femtosecond laser pulses split a single pulse into two subpulses, affecting electron interaction and ionization, ultimately regulating the C-cluster density in the plasma, an essential factor in twin GQD nucleation[76]. Temperature remains relatively stable during ablation, allowing for controlled crystallinity.

Controllable synthesis of twin GQDs is achieved through ETLAL of graphene dispersion. Laser parameters, especially temporally-shaped femtosecond pulses, control Coulomb explosion, affecting cavitation bubble composition. An external electric field enhances temperature and pressure, increasing collision probability and yielding twin GQDs. In ETLAL-based GQD preparation, pulse shaping influences size and layer count, while the electric field impacts crystal structure. Controlling the synthesis of twin GQDs was accomplished by adjusting electric fields and femtosecond laser parameters. It highlights that (1) Coulomb explosion in laser ablation generates the primary source of polycrystalline nanocrystal nuclei, increasing twin GQD proportions. (2) This approach effectively directs cavitation bubble movement, allowing crystal nuclei collisions at higher temperatures and pressures, critical for twin GQD formation. (3) Simultaneously, laser ablation and electric field ionization produce oxygen-containing functional groups that modify unsaturated carbon atoms on the edges and grain boundaries of twin GQDs. This offers a swift and eco-friendly method for efficiently preparing twin QDs, contributing to 2D material crystallization and defect engineering.

4. $MoSe_2$ 2H/1T hybrid nanoparticles

Hybrid nanoparticles of $MoSe_2$ in the 2H/1T phases are synthesized by femtosecond laser ablation of MoSe2 powder in isopropyl alcohol using varying laser powers and ablation durations, with a focus on understanding the mechanisms underlying their formation[78]. In contrast to other methods, which involved long-duration, high-power femtosecond laser ablation of TMDC powders in liquid for over 30 minutes, the spherical nanoparticles could be produced through either short-duration ablation at high power or extended ablation at low power. This onion-like nanoparticle exhibits a layered shell and an amorphous core, a structure that has been documented in prior studies utilizing nanosecond lasers for ablating MoS_2 bulk materials.

In Figure 9, the production yields of nanoparticles, synthesized at a constant ablation duration of 10 minutes with varying laser powers, are depicted. The production yield is determined by the ratio of the synthesized nanoparticle weight to the original powder weight. The weight of the nanoparticles was quantified using light absorbance in adherence to the Beer-Lambert law[79], following centrifugation to eliminate residual powder. It's noteworthy that the production yield demonstrated an increase with escalating laser power, reaching saturation.

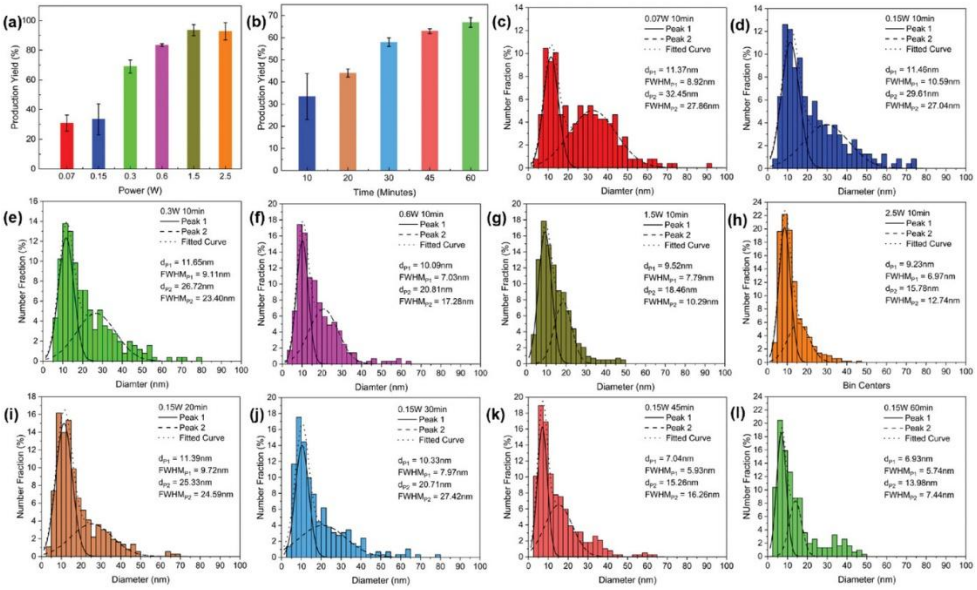

Figure 9: a,b) The production yields of $MoSe_2$ nanoparticles generated through laser ablation at varying power levels for 10 minutes (a) and $MoSe_2$ nanoparticles produced by laser ablation at a constant power of 0.15 W for different ablation durations (b). c–l) The size distributions of nanoparticles formed through laser ablation at 0.07 W for 10 minutes (c), 0.15 W for 10 minutes (d), 0.3 W for 10 minutes (e), 0.6 W for 10 minutes (f), 1.5 W for 10 minutes (g), 2.5 W for 10 minutes (h), 0.15 W for 20 minutes (i), 0.15 W for 30 minutes (j), 0.15 W for 45 minutes (k), and 0.15 W for 60 minutes (l), Reproduced from Wiley: Advanced materials with permission [78].

The observed trend aligns with filament length, indicating that a greater laser ablation area correlates with a heightened production yield. Notably, the highest yield, reaching 93%, was attained with laser powers of 1.5 W and 2.5 W, affirming the efficiency of the PLAL method in nanoparticle synthesis. During the process, powder particles were observed to circulate around the central location of the laser beam, positioned at the vial's center. It was evident that larger particles had a diminished likelihood of being ablated by the laser beam, primarily because they were more susceptible to circulating further from the vial's center due to the amplified centrifugal force. The observed plateau in production yield, beyond the 1.5 W laser power level, is likely attributed to the challenge of achieving comprehensive ablation of certain large powder particles within the relatively brief 10-minute timeframe. This phenomenon may have hindered the production yield from continuing to increase. In Figure 9c–h, the size distributions of nanoparticles synthesized over 10-minute duration at various laser powers are depicted. These samples exhibited a bimodal size distribution pattern, characterized by two distinct populations. The first group comprised smaller nanoparticles with narrow size dispersion (Peak 1), while the second group consisted of larger nanoparticles displaying broader size dispersion (Peak 2). To examine the impact of laser ablation time on $MoSe_2$ nanoparticle properties, $MoSe_2$ powder was ablated at a relatively low power of 0.15 W (to prevent significant oxidation) for durations of 10, 20, 30, 45, and 60 minutes. The results revealed that production yield increased with ablation time (Figure 9b), peaking at

69% for the 60-minute sample. Size distributions of nanoparticles synthesized at 0.15 W for various ablation times are shown in Figure 9 d, i–l.

Here two distinct types of spherical nanoparticles are observed: onion-structured nanoparticles, resulting from nucleation on melted droplet surfaces followed by inward growth of {002} planes of $MoSe_2$, and polycrystalline nanoparticles formed by the coalescence of crystalline nanoclusters fragmented from the powder during laser ablation. The nanoparticle size in the samples exhibits a bimodal distribution, reflecting different fragmentation mechanisms. The transition from the 2H to the 1T phase in the nanoparticles is likely due to electron doping from the laser-induced plasma [80]. Furthermore, the Photo-thermal conversion efficiencies (PTCEs)[80–82] of the nanoparticles increase with higher laser power and ablation time, with the highest PTCE reaching approximately 38%.

An investigation of the bandgaps and Urbach energies of these nanoparticles reveals that their elevated Photo-thermal conversion efficiencies (PTCEs) are predominantly linked to defects and structural disorder within the laser-synthesized nanoparticles. These imperfections enable the absorption of photons with energies below the bandgap energy and promote the non-radiative recombination of photoexcited carriers. This phenomenon underscores the significance of structural irregularities in enhancing the nanoparticles' light-absorption and energy conversion capabilities, shedding light on their potential for various applications.

5. MoS_2 QDs/GQDs.

The extensive interest in the field of electrocatalysis has been significantly fueled by the zero-dimensional quantum dots (QDs) of transition-metal dichalcogenides (TMDs) due to their exceptional characteristics, including superb catalytic activity, abundant catalytically active sites, size constraints, edge effects, and enhanced intrinsic conductivity[83].

MoS_2 quantum dots are highly promising catalysts for hydrogen evolution [84,85] due to their edge-related catalytic activity, resembling enzymatic centers with coordinative unsaturation. Additionally, the limited intrinsic conductivity of semiconducting 2H-MoS_2 QDs further hampers their HER performance, making it essential to boost both active site density and intrinsic conductivity to improve catalytic efficiency. Efforts to enhance the electrocatalytic properties of MoS_2 QDs have primarily focused on employing 2D/3D bulk materials, like combining 2H-MoS_2 QDs with graphene flakes, incorporating MoS_2 QDs with gold and embedding MoS_2 nanodots into NiNi Prussian blue analogue nanoplates. Reduced graphene oxide (rGO) has stood out as a well-explored choice in these studies due to its remarkable conductivity and substantial surface area, aiming to advance MoS_2 QD electrocatalysis. In electrocatalysis, rGO is a preferred support due to its high electrical conductivity and extensive surface area, while GQDs exhibit superior catalytic activity [86,87], particularly in hydrogen evolution reactions, offering the

potential for improved electrocatalytic processes with their edge-enhanced performance.

A highly efficient and precisely controlled approach is introduced for the one-step fabrication of closely interconnected 1T-2H MoS_2/N-rGO quantum-dot heterostructures through spatially shaped laser ablation in liquid (LAL)[88]. The process attains a remarkable QD yield of 75.16 wt%, affirming the practicality of mass-producing these quantum dots through the LAL method. This innovative technique demonstrates significant promise for scalable and controlled synthesis in the realm of quantum-dot heterostructures. To create MoS_2/N-rGO, the procedure involved directing a spatially shaped laser into a solution containing NH_3 through the use of a cylindrical lens, as depicted in Figure 10 [88]. Drawing from existing literature and the results of characterizations, a straightforward mechanism was established to explain the laser-assisted exfoliation and synthesis of tightly interconnected heterostructures. This mechanism provides insight into the processes involved in the preparation of these materials.

The samples exhibit a uniform distribution pattern. The heterostructures' thickness measures approximately 1.2 nm, give successful exfoliation of MoS_2 and GO to monolayer form and establishing a well-matched interface between MoS_2 QDs and rGO QDs. This phenomenon underscores the LAL method's ability to promote charge transfer and foster the creation of strongly interconnected quantum dot (QDs) heterostructures. Utilizing Gaussian light for this preparation method displays lower efficiency due to a smaller laser irradiation area at the same laser fluence, potentially leading to reduced hydrogen evolution reaction (HER) performance. The significant benefits of laser-assisted exfoliation and its effectiveness in controlling morphology.
The assembly of a 0D/0D heterojunction combining MoS_2 quantum dots (QDs) and graphene quantum dots (GQDs) holds significant promise for advanced electrocatalysis by capitalizing on the strengths of both materials. This junction optimizes the electronic configuration at the interface of MoS_2 QDs and GQDs while simultaneously enhancing the catalyst's electrical conductivity through their synergistic effects. Additionally, it is widely established that the metallic 1T-phase MoS_2 outperforms the semiconducting 2H-phase, primarily due to an increased number of catalytic sites, encompassing both edge sites and catalytically active basal planes, along with improved electrical conductivity.

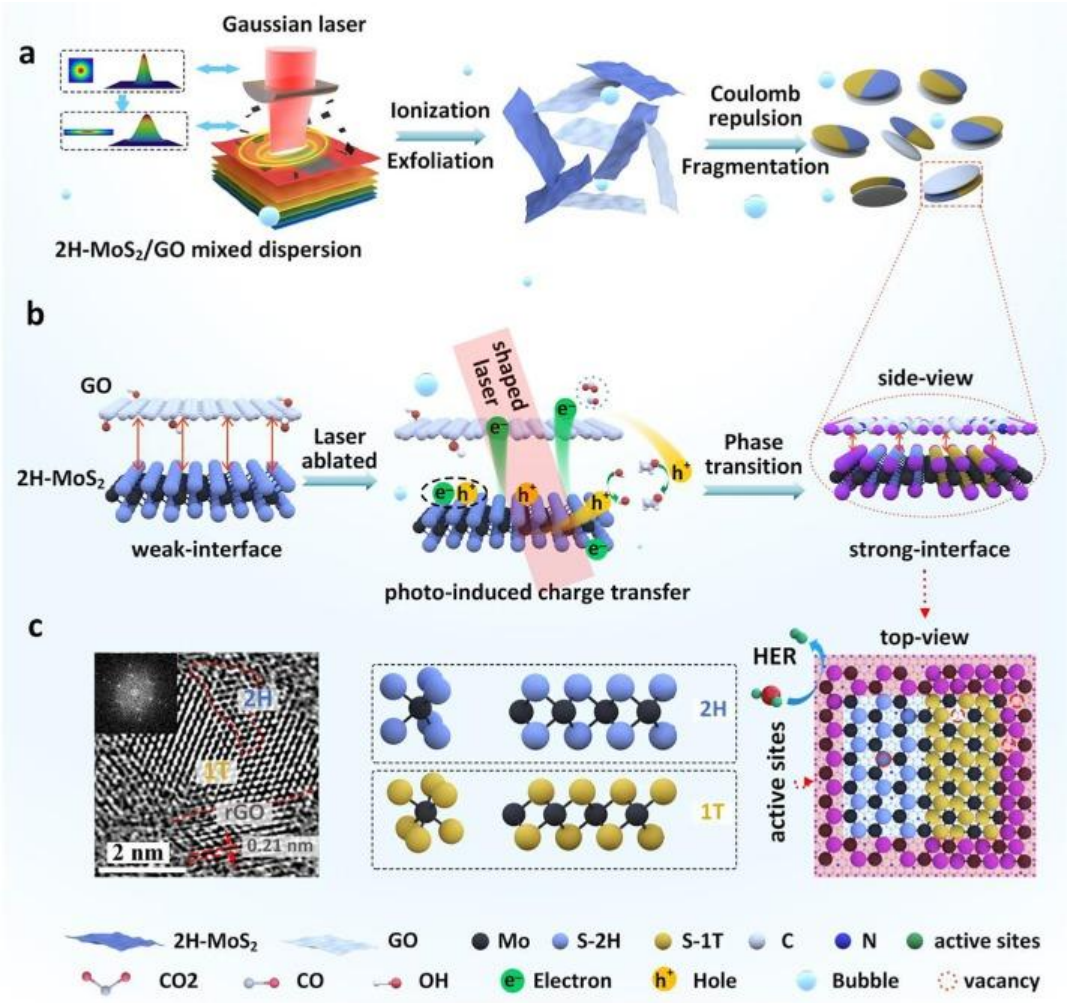

Figure 10: the formation mechanism of MoS_2/N-rGO quantum dots (QDs) heterostructures through a Laser Ablation in Liquid (LAL) process using a 2H-MoS_2/GO mixture. The LAL process involves plasma emission, exfoliation, and Coulomb repulsion, leading to local 2H-1T phase transitions in MoS2. The detailed reaction mechanism of MoS_2/N-rGO QDs prepared via LAL shows a photoinduced charge transfer process occurring at the heterostructure interface. Additionally, GO is reduced to rGO by the photogenerated electrons, while excess holes are neutralized by hydroxyl anions generated through laser ionization of ethanol molecules, strengthening the interlayer coupling between MoS_2 and rGO. These unique structures facilitate water splitting through a combination of morphology and electronic effects, with S atoms from different phases represented using distinct colors. High-resolution TEM (HRTEM) micrographs of C-MoS_2/N-rGO-0.65 and its simulated model are also depicted Reproduced from Elsevier: Chemical engineering with permission [88].

The incorporation of phase transition and a conductive support into 2H-MoS_2 quantum dots (QDs) is anticipated to enhance both the quantity of accessible active sites and the conductivity of these electrocatalysts, resulting in outstanding catalytic performance. However, despite these apparent advantages, conventional methods for creating 0D/0D heterojunctions can lead to slow hydrogen evolution reaction (HER) kinetics[89,90] due to stochastic physical interlayer connections and insufficient

modulation of the electronic structure. To overcome these challenges and optimize HER kinetics, further advancements in the design and fabrication of 0D/0D heterojunctions are necessary in the pursuit of efficient electrocatalysis.

6. MXene Quantum Dots/LRGO composite

Balancing the transparency of ultratransparent electrodes with their energy storage capacity has been a longstanding challenge in optoelectronics and energy technology[91,92]. To address this issue, a novel in-situ approach has been introduced, employing temporally and spatially shaped femtosecond laser technology to synthesize MXene quantum dots (MQDs). These MQDs are seamlessly integrated with laser-reduced graphene oxide (LRGO)[92], resulting in outstanding electrochemical capacitance without compromising ultrahigh transparency. This innovative technique holds significant potential for advancing transparent electrodes with improved energy storage capabilities, offering valuable applications in the realms of optoelectronics and energy technology.

Integrating unique MQDs into LRGO significantly boosts the electrode's specific surface area, benefiting from their nanoscale size and additional edge states[91]. The resulting MQD/LRGO supercapacitor demonstrates exceptional characteristics, including remarkable flexibility, durability, ultrahigh energy density, extended cycle life, and exceptional capacitance Furthermore, it maintains high transparency while delivering superior performance. MXenes, a category of 2D materials, have been extensively explored for energy storage applications due to their distinctive qualities. These include their intrinsic structure facilitating rapid ion transport and electron supply to electrochemically active sites, environmentally friendly properties, strong security features, and high specific capacitance. Nanometer-scale gaps resulting from material fragmentation significantly enhance transparency. Quantum dots (QDs), with their nanoscale diameters and favorable optical properties, are highly transparent materials. Moreover, their extensive specific surface area (SSA) and accessible edges make QDs excellent electrode materials for supercapacitors, as evidenced by multiple studies.

A temporally and spatially shaped femtosecond laser method is used to create transparent, flexible supercapacitors by fabricating MXene quantum dot (MQD) and laser-reduced graphene oxide (LRGO) composites, achieving both excellent electrochemical performance and transparency. Using a temporally and spatially shaped femtosecond laser, MXene target immersed in a GO dispersion is ablated, resulting in a one-step preparation of a transparent composite electrode. This technique employs a specific pulse delay (0–15 ps) with a Bessel-shaped laser (TSBL) focused on the MXene target, leading to plasma emission. Subsequent laser pulses continually ablate newly generated particles, reducing particle size, ensuring uniformity, and promoting dispersion.

Furthermore, the TSBL has 3D spatial features and an extended focusing range along the Z-axis, allowing for more effective ablation of the GO dispersion. This unique TSBL, when temporally shaped, controls the multilevel photoexfoliation of MXenes and utilizes water photoionization-enhanced light absorption to generate MQDs. The spatial shaping enhances the uneven distribution of the Z-axis optical field, achieving hierarchical optical reduction of GO and exfoliation. Unlike conventional Gaussian femtosecond lasers and temporally shaped Gaussian lasers, the TSBL beam enables the in-situ synthesis of electrode materials across both temporal and 3D spatial dimensions, significantly enhancing processing quality and efficiency.

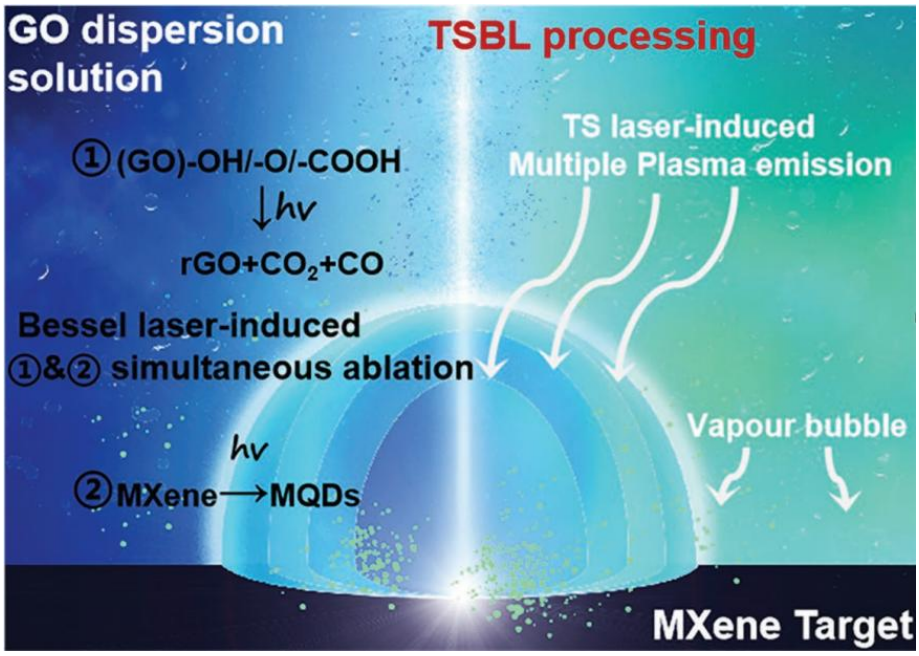

Figure 11: Schematic diagram showing the creation of MQD/LRGO composite materials with a close-up view of TSBL ablation on GO dispersions and MXene targets Reproduced from Wiley: Advanced materials with permission[91].

While laser ablating the composite materials, the colour of the solution progressively grew lighter. This change in colour resulted from material peeling and the quantization reaction initiated by the laser in the liquid phase. This reaction led to the reduction of GO nanosheets into LRGO with fewer layers and smaller particles.

Figure 11 shows a partially enlarged view of the laser ablation process for the composite material. The most intense TSBL energy interacted with the MXene target and initiated quantization, while lower laser energy above the focal point reduced the GO. In high-intensity laser-matter interactions, seed electrons are primarily produced by strong electric field ionization, involving multiphoton ionization and tunnelling ionization, initiated by the first subpulse. Excited electrons transition from bonding to antibonding states, weakening C - O electron bonding near the valence band's top, leading to the removal of oxygen atoms. Many free electrons are excited and gather in the GO suspension. The second subpulse aids the reduction process by providing

sufficient kinetic energy for oxygen atoms to exit the graphene sheet as gas, without significantly affecting carbon's kinetic energy.

Upon irradiation by the first subpulse, heated electrons are released from the MXene surface, and under the intense influence of the TSBL, plasma is emitted from the MXene target. This reduces interlayer interactions among MXene nanosheets, facilitating first-level photoexfoliation, leading to the creation of smaller, more uniform MQDs. Subsequently, electron-hole recombination on the MXene surface remains incomplete and enhanced ionization results in Coulomb repulsion among the nanosheets and MQDs. After the second temporally shaped femtosecond laser pulse (a few picoseconds later), ionization-induced charge accumulation strengthens Coulomb repulsion, promoting the emission of secondary plasma and the photoexfoliation of small monolayer MQDs.

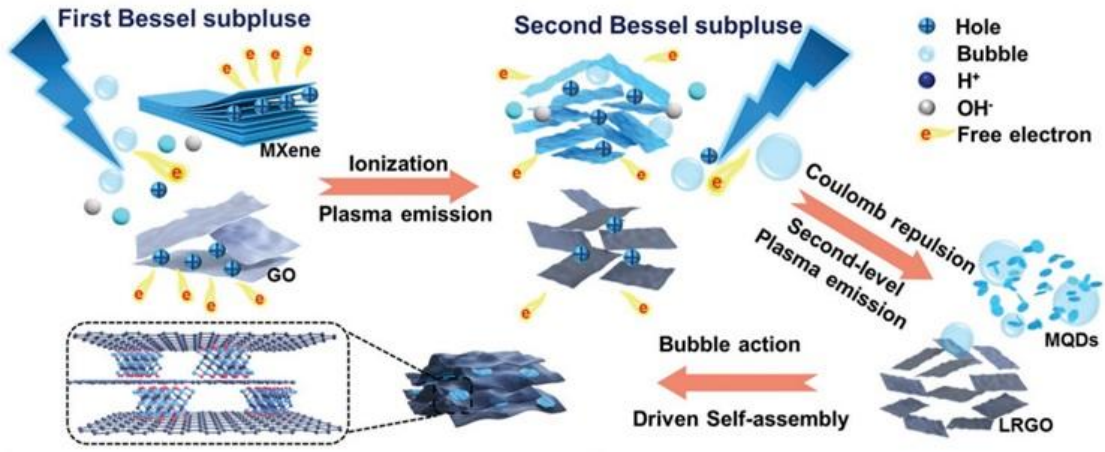

Figure 12: The comparison of the outcomes of three laser processes for MQD/LRGO composites and illustrates the detailed reaction mechanism for TSBL processing Reproduced from Wiley: Advanced materials with permission[91].

The results offers additional insights into the GO and MXene reaction process, demonstrating the creation of the MQD/LRGO composite, in line with the proposed mechanism[91]. It also compares the abilities of three lasers in synthesizing transparent composite electrode materials: TSBL, Gaussian laser, and temporally shaped Gaussian laser, labeled as TSBL-MQD/LRGO, GL-MQD/LRGO, and TL-MQD/LRGO. MQDs were evenly spread across the LRGO layer. The textured LRGO accommodated numerous MQDs on its surface and within folds, enhancing space utilization and preventing rGO self-stacking, thereby improving performance.

Conclusion

Femtosecond laser ablation is a straightforward and distinctive technique that overcomes limitations of conventional methods. It enables the creation of a wide range of functional nanomaterials from diverse solid materials and precursors in different solutions. By injecting energy in an extremely short period, ablation generates extreme

conditions with high temperature, pressure, and cooling rates, leading to the formation of various nanomaterials and other intriguing phenomena. Notable advantages of this approach include its versatility in producing a diverse array of nanostructures, as well as the high purity and in-situ dispersion and functionalization of the resulting nanomaterials in different solutions. This chapter aims to offer a comprehensive understanding of synthesis and the underlying mechanisms of femtosecond laser induced generation of variety of nanomaterials. It also provides a roadmap of the diverse nanomaterials attainable through this novel synthesis route and highlights their promising applications, serving as a foundation for future endeavours in this field.

Acknowledgement

The authors acknowledge the financial support from BRNS-DAE, Govt. of India, DST for funding through PURSE PII, FIST and Nano Mission programs, UGC, RUSA Major Research Projects 2.0, Govt. of India for funding through SAP-DRS and Innovative programs, SAIF-MGU and TEM-IIUCNN-MGU. We acknowledge CNRS for funding through International Emerging Actions between Institut Lumière Matière, CNRS, France and Mahatma Gandhi University, India

References

1. Hahn, David W., and Nicoló Omenetto. "Laser-induced breakdown spectroscopy (LIBS), part II: review of instrumental and methodological approaches to material analysis and applications to different fields." Applied spectroscopy 66.4 (2012): 347-419.
2. Hahn, David W., and Nicoló Omenetto. "Laser-induced breakdown spectroscopy (LIBS), part I: review of basic diagnostics and plasma–particle interactions: still-challenging issues within the analytical plasma community." Applied spectroscopy 64.12 (2010): 335A-366A.
3. Fantoni, R., et al. "Methodologies for laboratory laser induced breakdown spectroscopy semi-quantitative and quantitative analysis—a review." Spectrochimica Acta Part B: Atomic Spectroscopy 63.10 (2008): 1097-1108.
4. Noll, Reinhard, et al. "Laser-induced breakdown spectroscopy—from research to industry, new frontiers for process control." Spectrochimica Acta Part B: Atomic Spectroscopy 63.10 (2008): 1159-1166.
5. Santos Jr, Dario, et al. "Laser-induced breakdown spectroscopy for analysis of plant materials: a review." Spectrochimica Acta Part B: Atomic Spectroscopy 71 (2012): 3-13.
6. Singh, Vivek Kumar, and Awadhesh Kumar Rai. "Prospects for laser-induced breakdown spectroscopy for biomedical applications: a review." Lasers in medical science 26 (2011): 673-687.

7. Michel, Anna PM. "Applications of single-shot laser-induced breakdown spectroscopy." Spectrochimica Acta Part B: Atomic Spectroscopy 65.3 (2010): 185-191.
8. Russo, Richard E., et al. "Laser ablation molecular isotopic spectrometry." Spectrochimica Acta Part B: Atomic Spectroscopy 66.2 (2011): 99-104.
9. Russo, Richard E., et al. "Laser ablation molecular isotopic spectrometry." Spectrochimica Acta Part B: Atomic Spectroscopy 66.2 (2011): 99-104.
10. Mao, Xianglei, et al. "Laser ablation molecular isotopic spectrometry: parameter influence on boron isotope measurements." Spectrochimica Acta Part B: Atomic Spectroscopy 66.8 (2011): 604-609.
11. Koch, Joachim, and Detlef Günther. "Review of the state-of-the-art of laser ablation inductively coupled plasma mass spectrometry." Applied Spectroscopy 65.5 (2011): 155A-162A.
12. Hergenröder, Roland, Ota Samek, and Vanja Hommes. "Femtosecond laser ablation elemental mass spectrometry." Mass Spectrometry Reviews 25.4 (2006): 551-572.
13. Hergenröder, Roland. "Laser-generated aerosols in laser ablation for inductively coupled plasma spectrometry." Spectrochimica Acta Part B: Atomic Spectroscopy 61.3 (2006): 284-300.
14. R.E. Russo, J. Gonzalez, and C. Liu, LabPLus International (2006).
15. Becker, J. Sabine. "Recent developments in isotope analysis by advanced mass spectrometric techniques plenary lecture." Journal of analytical atomic spectrometry 20.11 (2005): 1173-1184.
16. Günther, Detlef, and Bodo Hattendorf. "Solid sample analysis using laser ablation inductively coupled plasma mass spectrometry." TrAC Trends in Analytical Chemistry 24.3 (2005): 255-265.
17. Russo, R. E., et al. "Laser assisted plasma spectrochemistry: laser ablation." Journal of Analytical Atomic Spectrometry 19.9 (2004): 1084-1089.
18. Hattendorf, Bodo, Christopher Latkoczy, and Detlef Günther. "Peer reviewed: laser ablation-ICPMS." (2003): 341-A.
19. Günther, Detlef. "Laser-ablation inductively-coupled plasma mass spectrometry." Analytical and bioanalytical chemistry 372 (2002): 31-32.
20. Russo, Richard E., et al. "Laser ablation in analytical chemistry—a review." Talanta 57.3 (2002): 425-451.
21. Nancy, Parvathy, et al. "Laser, nanoparticles, and optics." Nano-Optics. Elsevier, 2020. 47-65.

22. Rink, K., G. Delacrétaz, and R. P. Salathé. "Fragmentation process induced by microsecond laser pulses during lithotripsy." *Applied physics letters* 61.3 (1992): 258-260.

23. Stuart, Brent C., et al. "Optical ablation by high-power short-pulse lasers." *JOSA B* 13.2 (1996): 459-468.

24. Singh, S. C., et al. "Optical properties of selenium quantum dots produced with laser irradiation of water suspended Se nanoparticles." *The Journal of Physical Chemistry C* 114.41 (2010): 17374-17384.

25. Hu, Sheng-Liang, et al. "One-step synthesis of fluorescent carbon nanoparticles by laser irradiation." *Journal of Materials Chemistry* 19.4 (2009): 484-488.

26. Si, Jinhai, and Kazuyuki Hirao. "Phase-matched second-harmonic generation in cross-linking polyurethane films by thermal-assisted optical poling." *Applied Physics Letters* 91.9 (2007).

27. Cui, Wei, et al. "Compact bending sensor based on a fiber Bragg grating in an abrupt biconical taper." *Optics Express* 23.9 (2015): 11031-11036.

28. Nguyen, Vanthan, et al. "Femtosecond laser-induced size reduction of carbon nanodots in solution: Effect of laser fluence, spot size, and irradiation time." *Journal of Applied Physics* 117.8 (2015).

29. Amendola, Vincenzo, et al. "Top-down synthesis of multifunctional iron oxide nanoparticles for macrophage labelling and manipulation." *Journal of Materials Chemistry* 21.11 (2011): 3803-3813.

30. Xiao, J., et al. "Ultrahigh relaxivity and safe probes of manganese oxide nanoparticles for in vivo imaging." *Scientific reports* 3.1 (2013): 3424.

31. Amendola, Vincenzo, et al. "Magneto- plasmonic Au- Fe alloy nanoparticles designed for multimodal SERS- MRI- CT imaging." *Small* 10.12 (2014): 2476-2486.

32. Wagener, Philipp, et al. "Solvent-surface interactions control the phase structure in laser-generated iron-gold core-shell nanoparticles." *Scientific reports* 6.1 (2016): 23352.

33. Liu, Yongli, et al. "Hydrothermal synthesis of fluorescent carbon dots from sodium citrate and polyacrylamide and their highly selective detection of lead and pyrophosphate." *Carbon* 115 (2017): 550-560.

34. Liu, Wen, et al. "Green synthesis of carbon dots from rose-heart radish and application for Fe3+ detection and cell imaging." *Sensors and Actuators B: Chemical* 241 (2017): 190-198.

35. Xu, Huanhuan, et al. "One-step synthesis of nitrogen-doped carbon nanodots for ratiometric pH sensing by femtosecond laser ablation method." *Applied Surface Science* 414 (2017): 238-243.

36. Gu, Wei, et al. "A facile and one-step ethanol-thermal synthesis of MoS 2 quantum dots for two-photon fluorescence imaging." *Journal of Materials Chemistry B* 4.1 (2016): 27-31.

37. Perry, M. D., et al. "Ultrashort-pulse laser machining of dielectric materials." *Journal of applied physics* 85.9 (1999): 6803-6810.

38. Gamaly, Eugene G., et al. "Electrostatic mechanism of ablation by femtosecond lasers." *Applied surface science* 197 (2002): 699-704.

39. Maine, P., et al. "Generation of ultrahigh peak power pulses by chirped pulse amplification." *IEEE Journal of Quantum electronics* 24.2 (1988): 398-403.

40. Squier, Jeff, et al. "100-fs pulse generation and amplification in Ti: Al 2 O 3." *Optics letters* 16.5 (1991): 324-326.

41. Luther-Davies, B., et al. "Matter in ultrastrong laser fields." *Soviet journal of quantum electronics* 22.4 (1992): 289.

42. Momma, Carsten, et al. "Precise laser ablation with ultrashort pulses." *Applied surface science* 109 (1997): 15-19.

43. Nolte, Stefan, et al. "Ablation of metals by ultrashort laser pulses." *JOSA B* 14.10 (1997): 2716-2722.

44. Stoian, R., et al. "Coulomb explosion in ultrashort pulsed laser ablation of Al 2 O 3." *Physical review B* 62.19 (2000): 13167.

45. Bulgakova, Nadezhda M., et al. "Modeling of electron dynamics in laser-irradiated solids: Progress achieved through a continuum approach and future prospects." *International Conference on Lasers, Applications, and Technologies 2007: Laser-assisted Micro-and Nanotechnologies*. Vol. 6732. SPIE, 2007.

46. Du, Detao, et al. "Laser- induced breakdown by impact ionization in SiO2 with pulse widths from 7 ns to 150 fs." *Applied physics letters* 64.23 (1994): 3071-3073.

47. Roeterdink, W. G., et al. "Coulomb explosion in femtosecond laser ablation of Si (111)." *Applied Physics Letters* 82.23 (2003): 4190-4192.

48. Barthélemy, O., et al. "Influence of the laser parameters on the space and time characteristics of an aluminum laser-induced plasma." *Spectrochimica Acta Part B: Atomic Spectroscopy* 60.7-8 (2005): 905-914.

49. Laville, S., et al. "Fluid modeling of the laser ablation depth as a function of the pulse duration for conductors." *Physical review E* 66.6 (2002): 066415.

50. Perez, Danny, and Laurent J. Lewis. "Ablation of solids under femtosecond laser pulses." *Physical review letters* 89.25 (2002): 255504.

51. Itina, T. E., et al. "Numerical study of ultra-short laser ablation of metals and of laser plume dynamics." *Applied Physics A* 79 (2004): 1089-1092.

52. Chen, J. K., and J. E. Beraun. "Modelling of ultrashort laser ablation of gold films in vacuum." *Journal of Optics A: Pure and Applied Optics* 5.3 (2003): 168.

53. Itina, Tatiana E., et al. "Mechanisms of nanoparticle formation by short laser pulses." *Photon Processing in Microelectronics and Photonics VI*. Vol. 6458. SPIE, 2007.

54. Hergenröder, Roland. "A model of non-congruent laser ablation as a source of fractionation effects in LA-ICP-MS." *Journal of Analytical Atomic Spectrometry* 21.5 (2006): 505-516.

55. Mao, Xianglei, et al. "Preferential vaporization and plasma shielding during nano-second laser ablation." *Applied surface science* 96 (1996): 126-130.

56. Tulej, Marek, et al. "Current progress in femtosecond laser ablation/ionisation time-of-flight mass spectrometry." *Applied Sciences* 11.6 (2021): 2562.

57. Niu, K. Y., et al. "Morphology control of nanostructures via surface reaction of metal nanodroplets." *Journal of the American Chemical Society* 132.28 (2010): 9814-9819.

58. Niu, K. Y., et al. "Hollow nanoparticles of metal oxides and sulfides: Fast preparation via laser ablation in liquid." *Langmuir* 26.22 (2010): 16652-16657.

59. Luo, Ningqi, et al. "A general top-down approach to synthesize rare earth doped-Gd 2 O 3 nanocrystals as dualmodal contrast agents." *Journal of Materials Chemistry B* 2.35 (2014): 5891-5897.

60. Tsuji, Takeshi, et al. "Nanosecond time-resolved observations of laser ablation of silver in water." *Japanese journal of applied physics* 46.4R (2007): 1533.

61. Petersen, Svea, and Stephan Barcikowski. "In situ bioconjugation: single step approach to tailored nanoparticle- bioconjugates by ultrashort pulsed laser ablation." *Advanced Functional Materials* 19.8 (2009): 1167-1172.

62. Nancy, Parvathy, et al. "Laser–plasma driven green synthesis of size controlled silver nanoparticles in ambient liquid." *Nano-Structures & Nano-Objects* 16 (2018): 337-346.

63. Nancy, Parvathy, et al. "Fluorescence and Nonlinear Optical Response of Graphene Quantum Dots Produced by Pulsed Laser Irradiation in Toluene." *Molecules* 27.22 (2022): 7988.

64. Nancy, Parvathy, et al. "Fabrication of silver-decorated graphene oxide nanohybrids via pulsed laser ablation with excellent antimicrobial and optical limiting performance." *Nanomaterials* 11.4 (2021): 880.

65. Nancy, Parvathy, et al. "In situ decoration of gold nanoparticles on graphene oxide via nanosecond laser ablation for remarkable chemical sensing and catalysis." *Nanomaterials* 9.9 (2019): 1201.

66. Nancy, Parvathy, et al. "Green synthesis of graphene oxide/Ag nanocomposites via laser ablation in water for SERS applications." *AIP Conference Proceedings*. Vol. 2100. No. 1. AIP Publishing, 2019.

67. Nancy, Parvathy, Sabu Thomas, and Nandakumar Kalarikkal. "Au-GO nanohybrids as SERS platforms fabricated via pulsed laser ablation." *AIP Conference Proceedings*. Vol. 2369. No. 1. AIP Publishing, 2021.

68. Xu, Yanmin, et al. "Fabrication of transition metal dichalcogenides quantum dots based on femtosecond laser ablation." *Scientific reports* 9.1 (2019): 2931.

69. Tan, Chaoliang, et al. "Recent advances in ultrathin two-dimensional nanomaterials." *Chemical reviews* 117.9 (2017): 6225-6331.

70. Kapatel, Sanni, Chandresh Mania, and C. K. Sumesh. "Salt assisted sonochemical exfoliation and synthesis of highly stable few-to-monolayer WS 2 quantum dots with tunable optical properties." *Journal of Materials Science: Materials in Electronics* 28 (2017): 7184-7189.

71. Yan, Yinghan, et al. "Facile synthesis of water-soluble WS2 quantum dots for turn-on fluorescent measurement of lipoic acid." *The Journal of Physical Chemistry C* 120.22 (2016): 12170-12177.

72. Koromyslov, Sergei, et al. "Femtosecond Laser-Assisted Formation of Hybrid Nanoparticles from Bi-Layer Gold–Silicon Films for Microscale White-Light Source." *Nanomaterials* 12.10 (2022): 1756.

73. Ibrahim, Khaled H., et al. "A Novel Femtosecond Laser- Assisted Method for the Synthesis of Reduced Graphene Oxide Gels and Thin Films with Tunable Properties." *Advanced Materials Interfaces* 3.14 (2016): 1500864.

74. Nee, Chen-Hon, et al. "Direct synthesis of nanodiamonds by femtosecond laser irradiation of ethanol." *Scientific Reports* 6.1 (2016): 33966.

75. X. Li et al., “Preparation of twin graphene quantum dots through the electric-field-assisted femtosecond laser ablation of graphene dispersions,” Carbon N. Y., vol. 185, pp. 384–394, 2021.

76. L. Di et al., “Cold plasma treatment of catalytic materials: a review,” J. Phys. D. Appl. Phys., vol. 54, no. 33, p. 333001, 2021.

77. F. Ye, A. Ayub, R. Karimi, S. Wettig, J. Sanderson, and K. P. Musselman, “Defect Rich MoSe2 2H/1T Hybrid Nanoparticles Prepared from Femtosecond Laser Ablation in Liquid and Their Enhanced Photothermal Conversion Efficiencies,” *Adv. Mater.*, p. 2301129, 2023.

78. P. Yuan, R. Wang, H. Tan, T. Wang, and X. Wang, “Energy transport state resolved Raman for probing interface energy transport and hot carrier diffusion in few-layered MoS2,” *Acs Photonics*, vol. 4, no. 12, pp. 3115–3129, 2017.

79. P. Cheng, K. Sun, and Y. H. Hu, “Mechanically-induced reverse phase transformation of MoS 2 from stable 2H to metastable 1T and its memristive behavior,” RSC Adv., vol. 6, no. 70, pp. 65691–65697, 2016.

80. Y. Yao, J. Zhou, Z. Liu, X. Liu, G. Fu, and G. Liu, “Refractory materials and plasmonics based perfect absorbers,” Nanotechnology, vol. 32, no. 13, p. 132002, 2021.

81. F. Gao, Y. Miao, H. Ma, T. Zhang, H. Fan, and L. Zhao, “Boosting the photothermal performance of vacancy-rich MoSe 2− x nanoflowers for photoacoustic imaging guided tumor chemo-photothermal therapy,” Nanoscale, vol. 13, no. 35, pp. 14960–14972, 2021.

82. C.-H. Chiu, Y.-T. Chen, and J.-L. Shen, “Quantum dots derived from two-dimensional transition metal dichalcogenides: synthesis, optical properties and optoelectronic applications,” *Nanotechnology*, vol. 34, no. 48, p. 482001, 2023.

83. B. Mohanty, A. Mitra, B. Jena, and B. K. Jena, “MoS_2 quantum dots as efficient electrocatalyst for hydrogen evolution reaction over a wide pH range,” *Energy & Fuels*, vol. 34, no. 8, pp. 10268–10275, 2020.

84. Q. Zhou et al., “A feasible and environmentally friendly method to simultaneously synthesize MoS2 quantum dots and pore-rich monolayer MoS2 for hydrogen evolution reaction,” Int. J. Hydrogen Energy, vol. 45, no. 1, pp. 433–442, 2020.

85. Z. Du, S. Shen, Z. Tang, and J. Yang, “Graphene quantum dots-based heterogeneous catalysts,” New Carbon Mater., vol. 36, no. 3, pp. 449–467, 2021.

86. Y. Wu et al., “Graphene quantum dots as a highly efficient electrocatalyst for lithium–oxygen batteries,” J. Mater. Chem. A, vol. 8, no. 42, pp. 22356–22368, 2020.

87. L. Ma et al., “One-step ultrafast laser induced synthesis of strongly coupled 1T-2H MoS2/N-rGO quantum-dot heterostructures for enhanced hydrogen evolution,” Chem. Eng. J., vol. 445, p. 136618, 2022.

88. X. Jia, W. Chen, Y. Li, X. Zhou, X. Yu, and Y. Xing, “Enhanced photoexcited carrier separation in Ta3N5/SrTaO2N (1D/0D) heterojunctions for highly efficient visible light-driven hydrogen evolution,” Appl. Surf. Sci., vol. 514, p. 145915, 2020.

89. K. Zhu et al., “A novel I-type 0D/0D ZnS/Ag6Si2O7 heterojunction for photocatalytic hydrogen evolution,” J. Phys. Chem. Solids, vol. 175, p. 111206, 2023.

90. A. Esteghamat and O. Akhavan, “Graphene as the ultra-transparent conductive layer in developing the nanotechnology-based flexible smart touchscreens,” Microelectron. Eng., vol. 267, p. 111899, 2023.

91. Y. Yuan et al., “Ultrafast shaped laser induced synthesis of MXene quantum dots/graphene for transparent supercapacitors,” Adv. Mater., vol. 34, no. 12, p. 2110013, 2022.

92. X.-C. Han, Q. Wang, Z.-D. Chen, H. Zhou, Q. Cai, and D.-D. Han, “Laser-reduced graphene oxide for a flexible liquid sliding sensing surface,” *Opt. Lett.*, vol. 48, no. 3, pp. 839–842, 2023.